

Statistics of gamma-ray point sources below the *Fermi* detection limit

Dmitry Malyshev¹ and David W. Hogg

*Center for Cosmology and Particle Physics, New York University
4 Washington Place, Meyer Hall of Physics, New York, NY 10003, USA*

ABSTRACT

An analytic relation between the statistics of photons in pixels and the number counts of multi-photon point sources is used to constrain the distribution of gamma-ray point sources below the *Fermi* detection limit at energies above 1 GeV and at latitudes below and above 30°. The derived source-count distribution is consistent with the distribution found by the *Fermi* collaboration based on the first *Fermi* point source catalogue. In particular, we find that the contribution of resolved and unresolved active galactic nuclei (AGN) to the total gamma-ray flux is below 20 to 25%. In the best fit model, the AGN-like point source fraction is $17 \pm 2\%$. Using the fact that the Galactic emission varies across the sky while the extra-galactic diffuse emission is isotropic, we put a lower limit of 51% on Galactic diffuse emission and an upper limit of 32% on the contribution from extra-galactic weak sources, such as star-forming galaxies. Possible systematic uncertainties are discussed.

Keywords: galaxies: active; gamma rays: diffuse background; gamma rays: general; methods: statistical; quasars: general

¹dm137 at nyu.edu

On leave of absence from ITEP, Moscow, Russia, B. Cheremushkinskaya 25

1. Introduction

Faint gamma-ray point sources cannot be detected individually, however their presence affects the statistics of photons across the sky. One can use the observed statistics of photons to infer some general properties about the population of point sources below the *Fermi* detection limit. The idea of using the statistics of photon counts or intensity maps in the study of faint point sources is familiar in radio and X-ray observations (e.g., Scheuer 1957; Condon 1974; Scheuer 1974; Hasinger et al. 1993; Miyaji & Griffiths 2002; Softan 2011). A closely related subject is the use of extreme statistics to constrain the non-Gaussianity of cosmic microwave background data, e.g., Colombi et al. (2011) and references therein. In this paper, we extend the prior analysis (Slatyer & Finkbeiner 2010) and use the points in cells statistics to understand the population of gamma-ray point sources.

In a larger context, the problem is to separate different sources of gamma-ray emission. The standard strategy is either to use templates (Dobler et al. 2010) that trace the sources or else to simulate the cosmic ray propagation and gamma-ray production using, e.g., Galprop (Strong et al. 2007, 2009). In this paper we would like to adopt a different methodology: we assume some general properties of the sources in order to obtain model-independent constraints on the contribution from these sources.

We separate the sources based on their statistical properties. In the paper we consider three sources of gamma-rays at high latitudes. The first source is a diffuse source that varies over large angles. The main contribution to this source comes from the Galactic diffuse emission (π^0 production, ICS photons, and bremsstrahlung) and, possibly, a population of faint Galactic point sources, such as millisecond pulsars (Faucher-Giguère & Loeb 2010; Malyshev et al. 2010; ?). We will call this source non-isotropic Galactic diffuse emission. It puts a lower limit on the actual Galactic emission.

The second source corresponds to an isotropic distribution of gamma-rays, i.e., the statistics of photons across the sky is consistent with the Poisson distribution for this source. The isotropic flux has contributions from the homogeneous part of the Galactic diffuse emission, from diffuse intergalactic emission (references can be found in Stecker & Venters 2010), and from a population of very weak extragalactic sources that on average emit much less than one photon during the time of observation, such as star-forming galaxies (e.g., Pavlidou & Fields 2002; Fields et al. 2010), starburst galaxies (Thompson et al. 2007), galaxy clusters (Berrington & Dermer 2003), etc. The value of the isotropic emission puts an upper limit on the gamma-ray flux from very weak extra-galactic sources, as well as an upper limit on the contamination from cosmic rays (Abdo et al. 2010b).

The third source is a population of point sources modeled by a broken power-law source-count distribution. We assume that the point sources are distributed homogeneously over the sky. The statistics of photons coming from these point sources has a non-trivial form (derived in Appendix A) different from the Poisson statistics. These sources model a population of AGN-like point sources (Stecker et al. 1993; Padovani et al. 1993; Chiang et al. 1995; Stecker & Salamon 1996; Mücke & Pohl 2000; Abazajian et al. 2010; Neronov & Semikoz 2011).

We note that in our approach it is impossible to separate the isotropic part of Galactic emission from the diffuse extragalactic background (EGB). Consequently, all results will be quoted either with respect to the total gamma-ray flux or in absolute values. We find that at high latitudes (below and above 30°) for energies above 1 GeV the contribution of AGN-like point sources (both resolved and unresolved) to the total gamma-ray flux is $17\% \pm 2\%$, the contribution from Galactic diffuse emission is above 51% and the contribution from extra-galactic weak sources is below 32%. Using these values, we estimate that the contribution of unresolved AGN-like point sources to the EGB model in Abdo et al. (2010b) is below $\sim 25\%$, which is consistent with Abdo et al. (2010c).

The paper is organized as follows. In Section 2, we describe a general model and a fitting algorithm. In Section 3, we present an analysis of the *Fermi* data. Section 4 has discussion. In Appendix A, we derive the statistics of photons coming from a population of point sources. In Appendix B, we determine a model for non-isotropic Galactic diffuse emission. In Appendix C, we repeat the data analysis of Section 3 for different pixel sizes.

2. Model

In this section we describe the model that we later use to fit the *Fermi* gamma-ray data. At first, we present an analytic relation between the counts of photons in pixels and the statistics of point sources. Then we take into account the detector point spread function (PSF) and describe a model of Galactic diffuse gamma-ray emission. The model that we present in this section is rather general. An application of this analysis for the *Fermi* data is presented in Section 3.

2.1. Statistics of Photon Counts and Point Sources

We will assume a pixelation of the sphere with pixels of equal area. Usually a model of gamma-ray emission is represented in terms of the expected number x_p of gamma-rays in pixel p . The problem is that the number and the positions of weak point sources are not known. The

position of a point source can be found only by a “detection” of the source. However, if one is interested only in the total number of sources of a given flux, then a “detection” of sources is not necessary. In this paper, we use the statistics of photon counts in pixels, in order to find the source-count distribution of point sources without actual identification of the sources.

In order to find the statistics of photon counts in pixels we calculate the total number of pixels n_k that contain k photons. In this calculation, the information about the position of the pixels on the sky is not preserved, but the remaining information may be sufficient to constrain general properties of the population of sources. There are two competing conditions for this method to work. On the one hand, there should be sufficiently many pixels to determine the statistics of photon counts, while, on the other hand, the size of the pixels cannot be too small compared to the PSF, otherwise the statistics corresponding to the presence of point sources cannot be distinguished from non-isotropic diffuse emission.

If the total number of pixels is N_{pix} and n_k is the observed number of pixels with k photons, then we can estimate the probability to find k photons in a pixel as

$$p_k = \frac{n_k}{N_{\text{pix}}}. \quad (1)$$

For large N_{pix} , the statistical uncertainty of n_k is approximately $\sqrt{n_k}$ (there is a small correction due to the fact that the total number of pixels is fixed, i.e., the process is multinomial). If there are no point sources and all the emission comes from an isotropic diffuse source, then the probability distribution p_k is the Poisson probability of getting k photons given the mean rate. In the presence of point sources the probability distribution is more complicated than the Poisson distribution. In the context of X-ray point sources, the probability distribution is called a $P(D)$ distribution (or a $P(D)$ diagram) and is usually computed with the help of Monte Carlo simulations (e.g., Miyaji & Griffiths 2002).

In this paper we find an analytic relation between the probability distribution of photon counts in pixels and the source-count distribution. We will use this relation to find a source-count distribution that has the best fit to the observed probability distribution determined in Equation (1).

In calculations we use the method of probability generating functions (an introduction can be found in, e.g., Hoel et al. 1971, Section 3.6). For a given discrete probability distribution p_k , $k = 0, 1, 2, \dots$, the corresponding generating function is defined as a power series in an auxiliary variable t

$$P(t) = \sum_{k=0}^{\infty} p_k t^k. \quad (2)$$

If the generating function $P(t)$ is known, then the probabilities p_k can be found by picking the coefficient in front of t^k , or, equivalently, by differentiating with respect to t

$$p_k = \frac{1}{k!} \left. \frac{d^k P(t)}{dt^k} \right|_{t=0}. \quad (3)$$

An important property of probability generating functions is that a sum of two independent random variables corresponds to a product of the corresponding probability generating functions (Hoel et al. 1971). For example, if there are two independent sources of gamma-rays on the sky, e.g., Galactic and extragalactic, then the probability generating function for the photon counts with the two sources overlaid is given by the product of probability generating functions corresponding to the two sources (see Appendix A for more details).

Let x_m denote the average number of sources inside a pixel that emit exactly m photons during the time of observation. Using the sum-product property of probability generating functions (Hoel et al. 1971, Section 3.6), we derive in Appendix A the following relation between the probability generating function for the photon counts and the expected number x_m of m -photon sources

$$\sum_{k=0}^{\infty} p_k t^k = \exp \left(\sum_{m=1}^{\infty} (x_m t^m - x_m) \right). \quad (4)$$

This formula provides an analytic relation between the expected numbers of m -photon sources and the statistics of photons in pixels. The probabilities p_k to observe k photons in a pixel are determined by expanding the right hand side of this equation and picking the coefficient in front of t^k .

If we substitute $t = e^{i\omega}$, then Equation (2) becomes a discrete Fourier transform analog of the probability characteristic functions (e.g., Hoel et al. 1971). The probability characteristic functions were extensively used in the study of radio point sources below detection limit (e.g., Scheuer 1957). Similarly to probability generating functions, the characteristic function for a sum of two independent random variables corresponds to a product of the two characteristic functions.

The statistics of point sources can be described in terms of the differential source counts as a function of flux S , denoted by dN/dS . One of the simplest forms for the source-count distribution is a broken power-law

$$\frac{dN}{dS} \sim \begin{cases} S^{-n_1}, & S > S_{\text{break}} \\ S^{-n_2}, & S < S_{\text{break}}, \end{cases} \quad (5)$$

where we have to require $n_1 < 2$ and $n_2 > 2$ in order to have a finite total flux¹.

Let S be an average flux from a source (normalized to give the number of photons during the time of observation). Then the probability to observe m photons from this source is

$$p_m(S) = \frac{S^m}{m!} e^{-S}. \quad (6)$$

If the sources are distributed isotropically, then the average number of m -photon sources inside a pixel is given by the Poisson probabilities for sources with flux S to emit m photons

$$x_m = \frac{\Omega_{\text{pix}}}{4\pi} \int_0^\infty dS \frac{dN}{dS}(S) \frac{S^m}{m!} e^{-S}, \quad (7)$$

where Ω_{pix} is the angular area of the pixel.

2.2. PSF

In the case of non-zero PSF a source in some pixel may contribute gamma-rays to nearby pixels as well. In order to correctly estimate the number of point sources of a certain strength, we need to know how often a gamma-ray from a source in one pixel is detected in a different pixel.

We can represent the effect of the PSF as a smearing of a point source over some area, so that the flux from the point source is split between several pixels. We determine the average properties of the flux splitting from Monte Carlo simulations. In the simulation, we assume that the profile of the PSF is Gaussian. In order to calculate the average splitting, we put n Gaussians at random positions on the sphere and integrate every Gaussian over the pixels to get a collection of fractions f_i , $i = 1, \dots, N_{\text{pix}}$, such that $f_1 + f_2 + \dots = 1$ (in practice, one can truncate at some minimal value of f). Denote by $\Delta n(f)$ the number of fractions for n Gaussians that fall within Δf , then the average distribution of fractions is defined as

$$\rho(f) = \left. \frac{\Delta n(f)}{n \Delta f} \right|_{\Delta f \rightarrow 0, n \rightarrow \infty}. \quad (8)$$

¹ A benchmark model is provided by a static universe filled homogeneously with sources that have intrinsic luminosity L_0 . The number of sources with flux larger than $S = \frac{L_0}{4\pi R^2}$ is $N(S' > S) \sim R^3 \sim S^{-1.5}$. The differential number count is $dN/dS \sim -S^{-2.5}$. Index $n = 2.5$ provides a benchmark value for differential source count at large S . A break or a cutoff at small flux (large distance to the source) is necessary given the finite size of the visible universe.

This distribution is normalized as

$$\int f \rho(f) df = 1. \quad (9)$$

The case of zero PSF corresponds to $\rho(f) = \delta(f - 1)$. Sums over fractions are substituted by the integral $\int \rho(f) df$. In particular, the contribution of point sources with intrinsic flux between S and $S + dS$ to the total number of m -photon sources is

$$dx_m = dN(S) \int df \rho(f) \frac{(fS)^m}{m!} e^{-fS}. \quad (10)$$

The expected number of m -photon sources inside a pixel including the effect of PSF is

$$x_m = \frac{\Omega_{\text{pix}}}{4\pi} \int_0^\infty dS \frac{dN}{dS}(S) \int df \rho(f) \frac{(fS)^m}{m!} e^{-fS}. \quad (11)$$

An example of the function $\rho(f)$ relevant for the data analysis in Section 3 is presented in Figure 1. If we rescale the integration variable S in Equation (11) by f , then the effect of the PSF can be represented as a change of the source-count function

$$\frac{dN}{dS}(S) \longrightarrow \frac{d\tilde{N}}{dS}(S) = \int df \frac{\rho(f)}{f} \frac{dN}{dS}(S/f). \quad (12)$$

The apparent number of sources with small fluxes in $\frac{d\tilde{N}}{dS}$ is larger than the corresponding number of physical sources in $\frac{dN}{dS}$ due to contribution from point sources in nearby pixels, whereas the apparent number of sources with large fluxes is smaller due to loss of the flux to nearby pixels. One can see the effect of PSF in Figure 2 on the right. On the same figure, we also plot the expected number of m -photon sources for discrete m , derived from $\frac{d\tilde{N}}{dS}$.

2.3. The Model

In Equation (4), the probabilities p_k and the average expected number of m -photon sources may depend on the position of the pixel. The quantity that we use is the averaged probability $p_k = \frac{n_k}{N_{\text{pix}}}$, where n_k is the number of pixels with k photons. The generating function for averaged probabilities is given by

$$\sum_{k=0}^{\infty} p_k t^k = \frac{1}{N_{\text{pix}}} \sum_{p=1}^{N_{\text{pix}}} \exp \left(\sum_{m=1}^{\infty} (x_m^p t^m - x_m^p) \right). \quad (13)$$

This form of the generating function can be used when the distribution of sources is not isotropic or the exposure is non-uniform. If the exposure is sufficiently uniform, then we may assume that

the distribution of extragalactic sources is independent of the pixel position and can be taken out of the sum over pixels. The diffuse emission corresponds to “one-photon” source density that depends on the pixel, $x_{\text{diff}}(\text{p})$. Thus, the expression on the right-hand side of Equation (13) can be split into a product

$$\frac{1}{N_{\text{pix}}} \sum_{\text{p}=1}^{N_{\text{pix}}} e^{x_{\text{diff}}^{\text{p}} t - x_{\text{diff}}^{\text{p}} + \sum_{m=1}^{\infty} (x_m t^m - x_m)} = \left(\frac{1}{N_{\text{pix}}} \sum_{\text{p}=1}^{N_{\text{pix}}} e^{x_{\text{diff}}^{\text{p}} t - x_{\text{diff}}^{\text{p}}} \right) \cdot e^{\sum_{m=1}^{\infty} (x_m t^m - x_m)} \quad (14)$$

The second term in the product on the right hand side corresponds to the isotropic distribution of AGN-like point sources

$$P(t) = \exp \left(\sum_{m=1}^{\infty} (x_m t^m - x_m) \right), \quad (15)$$

while the first term corresponds to diffuse emission or, indistinguishably, one-photon sources

$$D(t) = \frac{1}{N_{\text{pix}}} \sum_{\text{p}=1}^{N_{\text{pix}}} e^{x_{\text{diff}}^{\text{p}} t - x_{\text{diff}}^{\text{p}}}. \quad (16)$$

It is convenient to separate the diffuse emission into a non-isotropic part that puts a lower limit on Galactic diffuse emission and an isotropic part that consists of isotropic Galactic component and a possible population of weak extragalactic sources (additional to AGN-like sources)

$$x_{\text{diff}}^{\text{p}} = x_{\text{Gal}}^{\text{p}} + x_{\text{isotr}}. \quad (17)$$

The main problem with the non-isotropic diffuse emission is a variability on large scales (on small scales the variability in Galactic emission is subdominant to Poisson noise and variability due to the presence of undetected point sources). In Appendix B we construct a model for the non-isotropic component $x_{\text{Gal}}^{\text{p}}$ that varies on large scales. We mask the known point sources and use low multipole spherical harmonics in order to filter out the small-scale variations while preserving the large-scale ones. We add a constant to $x_{\text{Gal}}^{\text{p}}$ so that $\min(x_{\text{Gal}}^{\text{p}}) = 0$. In the following, the non-isotropic component of diffuse emission is fixed. The corresponding generating function is

$$G(t) = \frac{1}{N_{\text{pix}}} \sum_{\text{p}=1}^{N_{\text{pix}}} e^{x_{\text{Gal}}^{\text{p}} t - x_{\text{Gal}}^{\text{p}}}. \quad (18)$$

We denote the probability generating function for the isotropic emission as

$$I(t) = e^{x_{\text{isotr}} t - x_{\text{isotr}}}. \quad (19)$$

The total generating function for the probability distribution of photons in pixel is the product of the three components

$$\sum_{k=0}^{\infty} p_k t^k = P(t) \cdot G(t) \cdot I(t). \quad (20)$$

The parameters of the point-source distribution in Equation (5) and the level of the isotropic flux x_{isotr} are found from fitting the probability distribution given in Equation (20) to the observed probability distribution. The details of the fitting algorithm are presented in the next subsection.

This simple factorized form of the generating function is valid in every pixel. In general, this factorization is not possible if we take an average over pixels, unless at most one sources is non-isotropic and the other sources can be taken out of the average over pixels. The factorization leads to a significant simplification of calculations at the expense that, due to a variation in exposure, a part of isotropic EGB may be misinterpreted as a non-isotropic Galactic foreground. This effect is expected to be small, provided that the *Fermi*-LAT exposure is sufficiently uniform (Atwood et al. 2009). Another possible source of systematic uncertainty is that the distribution of galaxies in the local neighborhood of the Milky Way is non-uniform and a part of emission from these galaxies can be misinterpreted as Galactic emission.

2.4. Fitting Algorithm

The algorithm has two main parts:

1. Determine the non-isotropic part $x_{\text{Gal}}^{\text{p}}$ of Galactic diffuse emission. We mask the bright point sources and use low multipoles of spherical harmonics to find the variable part of the remaining flux (Appendix B). Then we add a constant such that $\min(x_{\text{Gal}}^{\text{p}}) = 0$. In the following $x_{\text{Gal}}^{\text{p}}$ is fixed, i.e. we do not vary this component in fitting the pixel counts.
2. Use pixel counts to find x_{isotr} and dN/dS . The source-count distribution has four parameters: normalization, break, and two indices. Together with the level of isotropic contribution, x_{isotr} , this gives five fitting parameters which we denote by $\alpha = (A, S_{\text{break}}, n_1, n_2, x_{\text{isotr}})$, where A denotes the normalization in the source-count distribution in Equation (5).

The model prediction for the pixel counts $\nu_k(\alpha)$ is determined by multiplying the right-hand side of Equation (20) by N_{pix}

$$N_{\text{pix}} \cdot P(t) \cdot G(t) \cdot I(t) = \sum_{k=0} \nu_k(\alpha) t^k. \quad (21)$$

The expected pixel counts $\nu_k(\alpha)$ are found by expanding the left-hand side of this equation in powers of t and picking the coefficient in front of t^k . Given the observed number of pixels n_k with k photons, the likelihood of $\nu_k(\alpha)$ is estimated by the Poisson probability

$$L_k = \frac{\nu_k^{n_k}}{n_k!} e^{-\nu_k}. \quad (22)$$

The overall likelihood of the model is estimated as

$$L(\alpha) = \prod_k \frac{\nu_k(\alpha)^{n_k}}{n_k!} e^{-\nu_k(\alpha)}. \quad (23)$$

Here the product is over the number of photons k , while the data are represented by the number of pixels n_k that contain k photons. This is different from a usual coordinate space fit of maps, where the product is over pixels and the data are the number of photons k_p in a pixel p .

We use this likelihood function to find the best-fit parameters α_* for a given set of observed pixel counts n_k . The significance of deviation of α from α_* can be estimated as

$$\frac{\sigma(\alpha)^2}{2} = \ln L(\alpha_*) - \ln L(\alpha). \quad (24)$$

In the case of large counts the likelihood is well approximated by the Gaussian distribution and $\sigma(\alpha)$ is the deviation in sigma values.

3. Data analysis

We consider 11 months of *Fermi* data (August 4, 2008 - July 4, 2009) that were used for the first *Fermi* point-source catalog (Abdo et al. 2010a) and for the *Fermi* analysis of the source-count distribution (Abdo et al. 2010c).

In order to reduce the PSF, we use front-converted gamma-rays, i.e., the gamma-rays converted in the front part of the *Fermi*-LAT tracker (Atwood et al. 2009), with energies between 1 GeV and 300 GeV. The corresponding (quadratic) average of the PSF is 0.4° .² For pixelation of data, we use HEALPix (Górski et al. 2005) with the pixelation parameter $n_{\text{side}} = 32$, which corresponds to pixel size about 2 degrees.³ We mask the galactic plane within 30 degrees in latitude. The number of pixels outside of the mask is $N_{\text{pix}} = 6178$ and the number of photons is 152,143.

The distribution of pixel counts is presented in Figure 2 on the left. We model this distribution by a combination of three components: non-isotropic Galactic diffuse emission derived in Appendix B, isotropic distribution of photons, and the distribution of AGN-like point sources described in Section 2.3. The best-fit models for the isotropic flux and the AGN-like point sources are presented in Figure 2 on the right.

² http://www-glast.slac.stanford.edu/software/IS/glast_lat_performance.htm

³ We consider the cases of $n_{\text{side}} = 16$ and $n_{\text{side}} = 64$ in Appendix C.

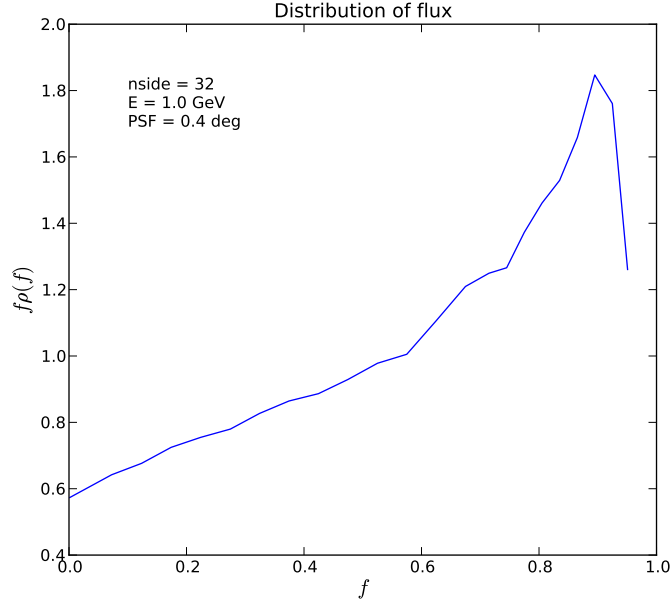


Fig. 1.— Average distribution of flux among pixels from Gaussian sources at random positions. The width of the Gaussian corresponds to the average point spread function for front-converted gamma-rays with energies between 1 GeV and 300 GeV. The pixels are determined in HEALPix (Górski et al. 2005) with $n_{\text{side}} = 32$. x -axis: fraction of the flux, y -axis: density of pixels as a function of f (cf., Equation (8)) multiplied by the flux fraction. The fractions are computed by taking 50,000 Gaussian distributions at random positions on the sphere. The area under the curve corresponds to the total flux equal to 1.

In fitting we consider pixel counts n_k with $k < 500$, i.e., the number of data points is $N_{\text{points}} = 500$. We use $\ell_{\text{max}} = 20$ for the Galactic diffuse emission model. The sampling is performed with Metropolis-Hastings Markov Chain Monte Carlo method with 1500 steps. The average model is presented in Figure 2 and compared with *Fermi* models in Table 1. We find that the position of the break is almost a flat direction. The results of fitting with a set of fixed break positions are presented in Figure 3.

We find that the contribution of point sources to the gamma-ray flux is $(17 \pm 2)\%$. This fraction is obtained by integrating the best-fit source-count model presented in Figure 2 and in Table 1 from zero to infinity. This fraction is not model independent, i.e., it may change for different shapes of the source-count function used in fitting, but, provided that the broken power-law source-counts distribution gives a good fit to the data, we do not expect a large systematic uncertainty due to the change in the shape of the fitting function. In part this can be justified by looking at the models with fixed positions of the break: most of the models in Figure 3 have the point-source fraction $q_{\text{ps}} \lesssim 0.25$.

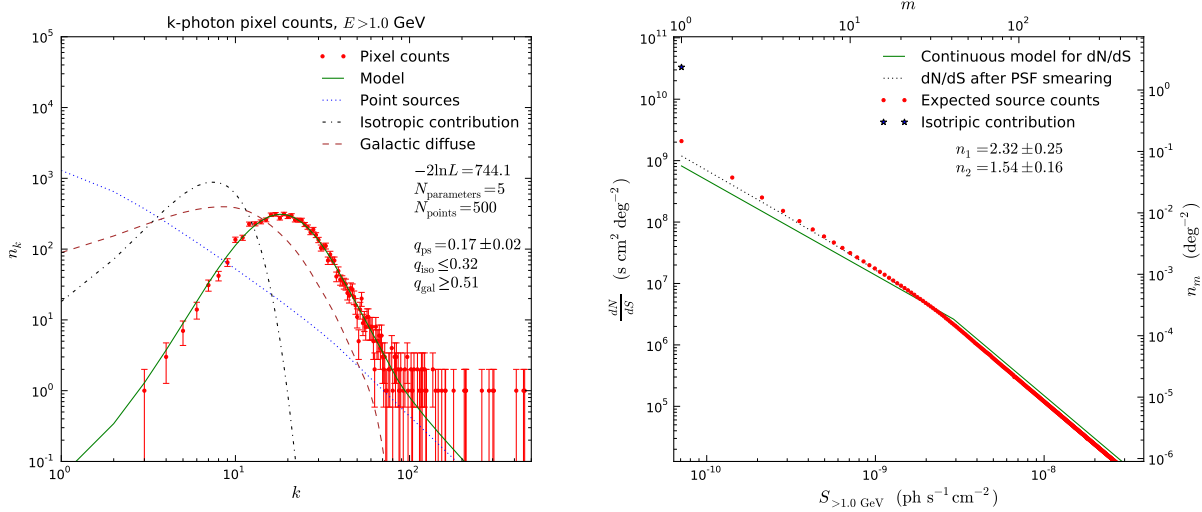


Fig. 2.— Left plot: n_k is the number of pixels with k photons, the red dots correspond to pixel counts derived from *Fermi* data, the errors bars are equal to $\sqrt{n_k}$. We consider three sources: AGN-like point sources (blue dotted line), isotropic Poisson contribution (brown dashed line), and non-isotropic Galactic diffuse emission (black dash-dotted line). Note, that the total model on this plot is not the sum of the components, the corresponding generating function of the PDF is a product of the generating functions in Equation (20). N_{points} corresponds to the number of points on the x -axis that we have used for fitting, $k < 500$. Right plot: green solid line is the physical model for the AGN-like source counts, blue dotted line is the source counts in pixels in the presence of PSF (Equation (12)), points represent expected number of m -photon sources per deg^2 as defined in Equation (11), blue star is the value of the isotropic flux.

At smaller position of the break the contribution of point sources becomes larger ($q_{\text{ps}} \sim 0.3$ for the left point in Figure 3) but the fit has smaller likelihood. It would be interesting to estimate constraints on models involving high redshift AGNs to explain the unresolved part of the EGB (e.g., Abazajian et al. 2010; Neronov & Semikoz 2011) using the statistics of photon counts.

We can also put an approximate lower bound of 51% on Galactic diffuse emission, and an approximate upper bound of 32% on isotropic emission consistent with Poisson statistics. In terms of the absolute flux values, the total gamma-ray flux above 1 GeV for $|b| > 30^\circ$ is $F_{\text{tot}} = 1.75 \times 10^{-6} \text{ s}^{-1} \text{cm}^{-2} \text{sr}^{-1}$, the diffuse Galactic flux is $F_{\text{Gal}} > 8.8 \times 10^{-7} \text{ s}^{-1} \text{cm}^{-2} \text{sr}^{-1}$, the isotropic component of the flux is $F_{\text{isotr}} = (5.6 \pm 0.6) \times 10^{-7} \text{ s}^{-1} \text{cm}^{-2} \text{sr}^{-1}$, the flux from AGN-like point sources with dN/dS parameters given in Table 1 and in Figure 2 is $F_{\text{PS}} = (3.0 \pm 0.4) \times 10^{-7} \text{ s}^{-1} \text{cm}^{-2} \text{sr}^{-1}$.

Using this value of the total flux from AGN-like point sources, we can estimate the gamma-

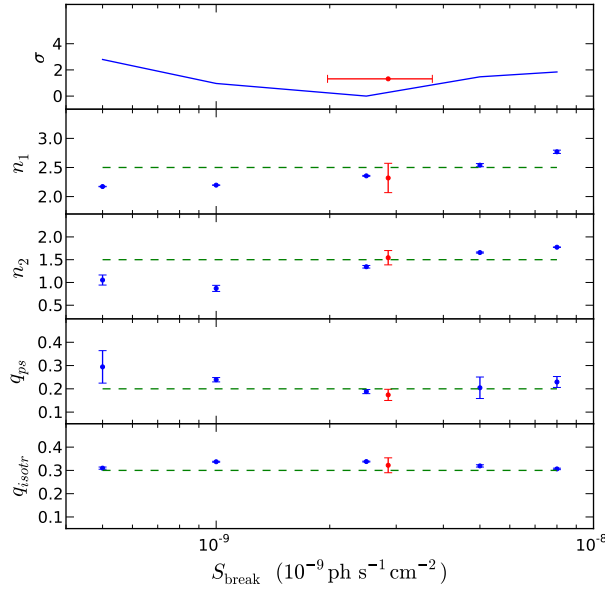


Fig. 3.— Results of fitting the AGN-like source-count distribution for fixed positions of the break. The significance of deviation is determined from Equation (24) as $\sigma = \sqrt{2\Delta \ln \bar{L}}$. n_1 and n_2 are the indices above and below the break for differential source-count distribution, q_{ps} is the fractional contribution from AGN-like point sources, q_{isotr} is the fractional contribution from an isotropic source (it provides an upper limit on the extra-galactic isotropic contribution additional to AGN-like point sources). Red dots correspond to the model used in Figure 2. Green dashed lines provide reference values: $n_1 = 2.5$, $n_2 = 1.5$, $q_{ps} = 0.2$, and $q_{isotr} = 0.3$.

ray flux from undetected sources. The total flux in the energy range 1 - 100 GeV from point sources at $|b| > 30^\circ$ detected by *Fermi* (Abdo et al. 2010a) is $F_{Fermi\ AGN} = 2.1 \times 10^{-7} \text{ s}^{-1} \text{ cm}^{-2} \text{ sr}^{-1}$. Consequently, the flux from undetected AGN-like point sources above 30° can be estimated as $F_{unres\ AGN} = 0.9 \times 10^{-7} \text{ s}^{-1} \text{ cm}^{-2} \text{ sr}^{-1}$. This value is reasonable, since from Figure 4 it follows that the detected point sources give a good approximation to the best-fit distribution of sources down to fluxes below the break in $N(S)$, while the contribution of point sources to the gamma-ray background is saturated around the break. The extragalactic diffuse emission can be estimated from the model presented in Abdo et al. (2010b). In this model, the EGB flux above 1 GeV is $F_{EGB} \approx 4 \times 10^{-7} \text{ s}^{-1} \text{ cm}^{-2} \text{ sr}^{-1}$. The contribution of unresolved AGN's to this EGB flux is about 23%. This value is consistent with the estimations in Abdo et al. (2010c). We would like to stress that our analysis is different from Abdo et al. (2010c). We do not count any sources, but rather do a “blind” statistical analysis. The consistency of results may serve as a non-trivial check of both methods.

Table 1: Comparison with *Fermi* Results (Abdo et al. 2010c).

Analysis	n_1	n_2	S_{break}^a
This work	2.31 ± 0.25	1.54 ± 0.16	2.9 ± 0.9
<i>Fermi</i> > 100 MeV	2.44 ± 0.11	1.58 ± 0.08	2.8 ± 0.5^b
<i>Fermi</i> 1 - 10 GeV	$2.38_{-0.14}^{+0.15}$	$1.52_{-1.1}^{+0.8}$	2.3 ± 0.6

^a In units of $10^{-9} \text{ph s}^{-1} \text{cm}^{-2}$.

^b Rescaled from the break in Abdo et al. (2010c) according to energy spectrum $\sim E^{-2.4}$.

4. Discussion

One of the most interesting problems in gamma-ray astrophysics is to understand the origin of EGB flux, which is defined as the total gamma-ray flux minus the contribution from resolved point sources, minus the Galactic foreground (Abdo et al. 2010b). In general, we can separate the sources of diffuse EGB into two big classes: non-Poisson sources and Poisson-like sources. In the first case, the contribution comes from sources below detection limit that may emit several photons during the observation time, these are the AGN-like point sources (e.g., Padovani et al. 1993; Chiang et al. 1995; Stecker & Salamon 1996; Abazajian et al. 2010; Neronov & Semikoz 2011). In this case the statistics of photon counts in pixels across the sky will be different from Poisson statistics due to correlation among photons coming from the same point source. In the second case, there is a large number of sources emitting on average much fewer than one photon during the observation time, e.g., star-forming and star-burst galaxies (Pavlidou & Fields 2002; Thompson et al. 2007; Fields et al. 2010). The statistics of photons in this case will be very close to Poisson statistics.

These two possibilities are relatively hard to separate based only on energy spectrum arguments (see, however, Abazajian et al. 2010; Stecker & Venters 2010; Neronov & Semikoz 2011). Alternatively, one can use a correlation between gamma-ray emission and multi-wavelength emission from AGNs (Urry & Padovani 1995; Mücke & Pohl 2000; Abdo et al. 2010d; Angelakis et al. 2010; Li & Cao 2011) together with AGN population studies (e.g., Padovani & Giommi 1995; Hopkins et al. 2007; Padovani et al. 2007; Rigby et al. 2008; Hodge et al. 2009; Smolčić et al. 2009) to infer the AGN contribution to gamma-ray background.

In this paper we show that the statistics of photons in pixels can also be used to constrain the distribution of point sources below the detection limit. We find that there is a slight preference for two populations of point sources: the AGN-like point sources with a break at relatively high flux and a population of faint sources such as star-forming galaxies rather than a single

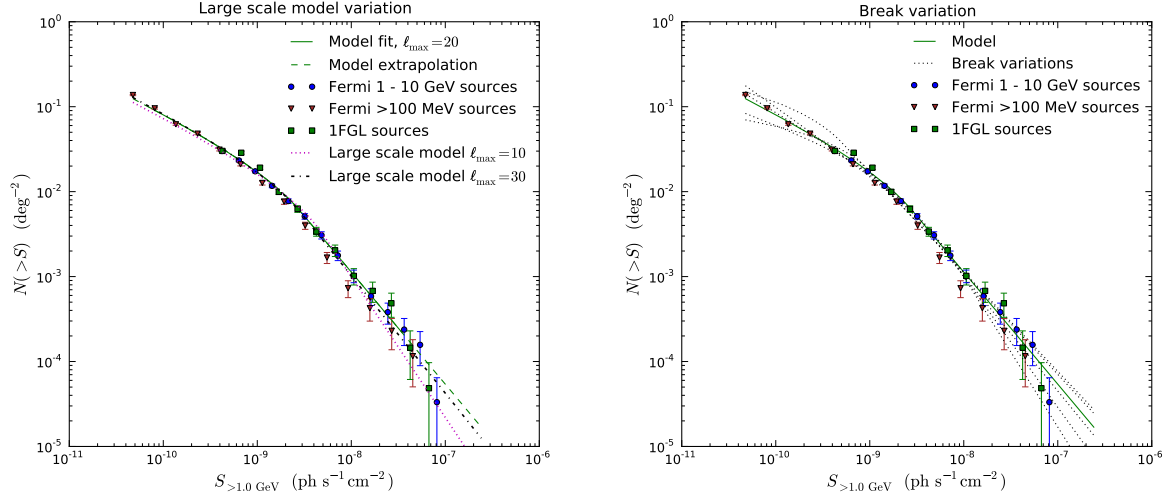


Fig. 4.— Left plot: different lines correspond to different models for Galactic diffuse emission of gamma-rays corresponding to $\ell_{\max} = 10, 20, 30$ (Appendix B). Solid green line corresponds to the range of photon counts (1 to 500) used in fitting. Dashed green line is the extrapolation of the model. Magenta triangles correspond to total source counts found by *Fermi* collaboration above 100 MeV (right plot in Figure 9 of Abdo et al. 2010c) with flux rescaled assuming energy density spectrum $\sim E^{-2.4}$. Blue circles correspond to sources found by the *Fermi* collaboration in 1 – 10 GeV energy bin (center plot in Figure 17 of Abdo et al. (2010c)). Green squares correspond to 1 – 100 GeV flux for sources in the first *Fermi* catalog (Abdo et al. 2010a). Right plot: models with different fixed positions of the break presented in Figure 3.

population of AGN-like point sources with a break at a smaller flux. This statement is insensitive to the energy spectrum since we use the integrated flux above 1 GeV but it may depend on the form of the function used to fit the point source number counts. Possible sources of systematic uncertainty include the source smearing due to PSF, non-isotropic Galactic diffuse emission, non-isotropic emission (on large scales) from nearby galaxies, and non-homogeneous exposure. The interpretation of the point-source number counts may also be affected by clustering of sources on scales smaller than the PSF.

A stronger constrain on the population of gamma-ray point sources may come from an unpixelized analysis of the data. In this more general analysis, the likelihood of a model depends on the full gamma-ray data (positions on the sky, energy, arrival time) rather than the counts of gamma-rays in pixels. This likelihood would have the form of an integral over flux times the source number counts, times an integral over all possible positions of the sources on the sky. The photon counts approximation is simpler computationally and already gives rough constraints on the source population, while the full unbinned analysis may provide stronger con-

straints at the expense of computational complexity. Examples of unbinned analysis using some part of gamma-ray data include the gamma-ray two-point correlation function (e.g., Ave et al. 2009; Geringer-Sameth & Koushiappas 2010), angular power spectrum (Ando & Komatsu 2006; Hensley et al. 2010), nearest neighbor statistics (Softan 2011), etc.

We also believe that the techniques of generating functions in the study of photon counts statistics, known for some time in radio and X-ray observations, may have further important applications in data analysis of current and future radio, IR, X-ray, and gamma-ray observations.

Acknowledgments.

The authors are thankful to Kevork Abazajian, Marko Ajello, Jo Bovy, Christopher Kochanek, Jennifer Siegal-Gaskins, Tracy Slatyer, Tonia Venters, and Itay Yavin for stimulating discussions and useful comments. We are also thankful to Ilias Cholis for the help in selecting the *Fermi* gamma-ray data. This work is supported in part by the Russian Foundation of Basic Research under Grant No. RFBR 10-02-01315 (D.M.), by the NSF Grant No. PHY-0758032 (D.M.), by Packard Fellowship No. 1999-1462 (D.M.), by NASA grant NNX08AJ48G (D.W.H.), and by the NSF grant AST-0908357 (D.W.H.). Some results in this paper have been obtained using the HEALPix package (Górski et al. 2005).

A. Derivation of statistics

In this Appendix we derive the photon counts statistics in the presence of point sources. The derivation is based on the following well known property of generating functions for probabilities: the generating function of a sum of two independent sources is the product of the corresponding generating functions (e.g., Hoel et al. 1971, Section 3.6). Indeed, consider a box where we can put red balls with probabilities p_k , $k = 1, 2, 3 \dots$, and blue balls with corresponding probabilities q_k , $k = 1, 2, 3 \dots$, then the probability to find k balls of any color is

$$r_k = \sum_{k'=0}^k p_{k'} q_{k-k'}, \quad k = 1, 2, 3 \dots \quad (\text{A1})$$

The last equation is the rule for multiplication of polynomials or power series. Let

$$R(t) = \sum_k r_k t^k, \quad P(t) = \sum_k p_k t^k, \quad Q(t) = \sum_k q_k t^k, \quad (\text{A2})$$

then

$$R(t) = P(t) \cdot Q(t). \quad (\text{A3})$$

As before, denote the probability to observe k photons in a pixel by p_k . The corresponding generating function is

$$P(t) = \sum_k p_k t^k. \quad (\text{A4})$$

The knowledge of the generating function is equivalent to the knowledge of all p_k , provided that every p_k can be found from $P(t)$ by picking the term in front of t^k .

We will now derive the generating function for probabilities to observe k photons from a collection of point sources. Denote by x_m the average number of point sources inside a pixel that emit exactly m photons during the time of observation. We assume that the probability to find n_m m -photon sources in a pixel is given by the Poisson statistics

$$p_{n_m}(x_m) = \frac{x_m^{n_m}}{n_m!} e^{-x_m}, \quad (\text{A5})$$

then the probability to find k photons from m -photon sources is

$$p_k^{(m)} = \begin{cases} p_{n_m}(x_m), & \text{if } k = m \cdot n_m \text{ for some } n_m; \\ 0, & \text{otherwise.} \end{cases} \quad (\text{A6})$$

The corresponding probability generating function is

$$P^{(m)}(t) = \sum_k p_k t^k = \sum_{n_m} t^{m \cdot n_m} \frac{x_m^{n_m}}{n_m!} e^{-x_m} = e^{x_m t^m - x_m}. \quad (\text{A7})$$

The generating function of probabilities p_k to observe k photons from any sources is the product of the generating functions for every m

$$\begin{aligned} \sum_{k=0}^{\infty} p_k t^k &= \prod_{m=1}^{\infty} e^{x_m t^m - x_m} \\ &= \exp \left(\sum_{m=1}^{\infty} (x_m t^m - x_m) \right). \end{aligned} \quad (\text{A8})$$

If we denote $t = e^{2\pi i \omega}$ and

$$\tilde{P}(\omega) = \sum_{k=0}^{\infty} p_k e^{2\pi i \omega k}, \quad (\text{A9})$$

$$\tilde{X}(\omega) = \sum_{m=0}^{\infty} x_m e^{2\pi i \omega m}, \quad (\text{A10})$$

then Equation (A8) can be represented as

$$\tilde{P}(\omega) = e^{\tilde{X}(\omega) - \tilde{X}(0)}, \quad (\text{A11})$$

which is the discrete Fourier transform analog of characteristic functions considered in, e.g., Scheuer (1957).

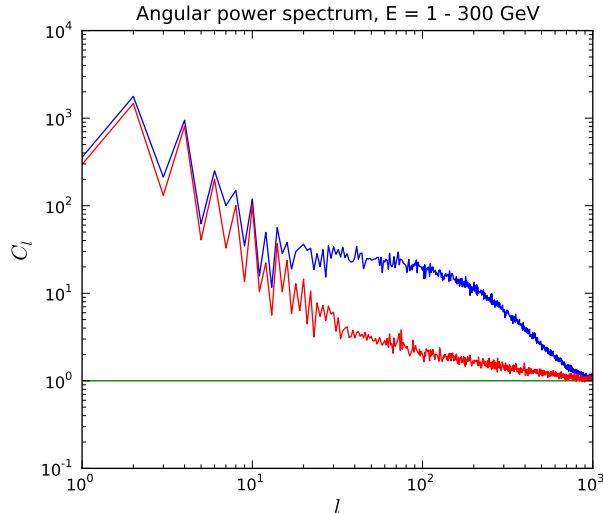


Fig. 5.— Blue line (upper): angular power spectrum of gamma-ray data with $|b| > 30^\circ$. Red line (lower): same as the blue line, but with additional masking of *Fermi* gamma-ray point sources (Figure 6). The normalization is chosen such that for the Poisson noise $\langle C_l \rangle = 1$ (constant green line). C_l 's below $\ell \sim 10$ are dominated by the variation in Galactic diffuse emission on large scales. Constant C_l 's above $\ell = 10$ are due to contribution of point sources. Decay of C_l 's above $\ell \sim 100$ for the blue line is due to detector PSF. In our case $\langle \text{PSF} \rangle \approx 0.4^\circ$, which corresponds to $\ell \gtrsim 400$. A smoothed model for large-scale structure distribution is obtained by spherical harmonics decomposition up to $\ell = 20$, the corresponding map of the model is presented in Figure 6.

B. Non-isotropic Galactic diffuse emission

In this appendix, we describe a model for the non-isotropic Galactic diffuse emission. This signal is “filtered” by low multipoles of the gamma-ray data. In this approach, the homogeneous part of Galactic emission is indistinguishable from extragalactic flux. Also some part of extragalactic emission from galaxies and galaxy clusters close to Milky Way may lead to a signal that varies over the sky and can be misinterpreted as non-isotropic Galactic emission. However, the majority of extragalactic emission comes from higher redshifts where the distribution of extragalactic sources is sufficiently uniform on large scales.

In Figure 5, we plot the angular power spectrum for the data at high latitudes ($|b| > 30^\circ$) before and after masking the point sources in the first *Fermi* catalog (Abdo et al. 2010a). The angular power spectrum is

$$C_l = \frac{1}{2l + 1} \sum_m |a_{lm}|^2, \quad (\text{B1})$$

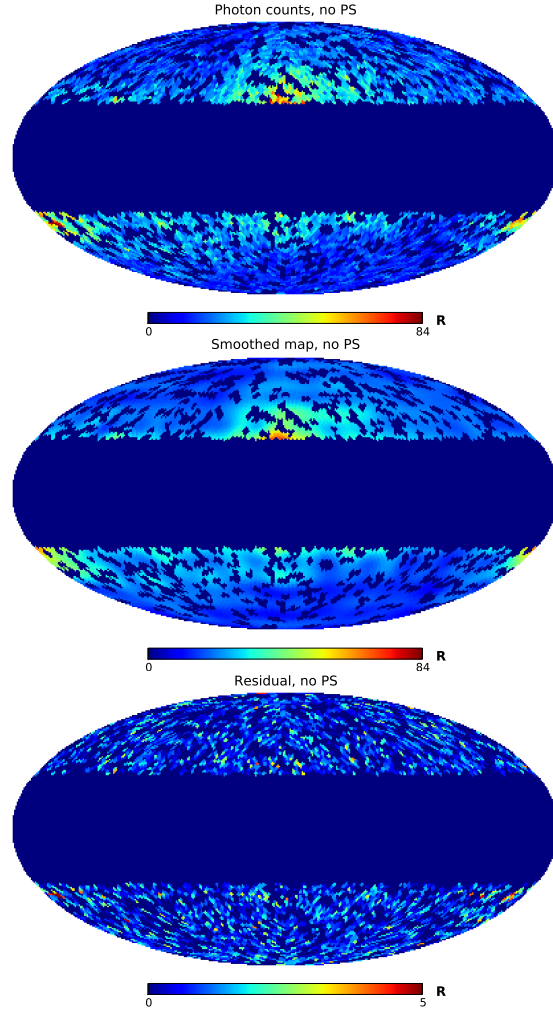


Fig. 6.— Sky maps for photon counts and for a Galactic diffuse emission model derived from the photon counts by using the spherical harmonics decomposition with $l \leq 20$ (Equation (B2)). Residuals are in sigma values: $\frac{|\text{model}-\text{data}|}{\sqrt{\text{model}}}$.

where a_{lm} 's are the spherical harmonics coefficients of $f(p) \cdot m(p)$, where $f(p)$ is the number of photon counts inside pixel p and $m(p)$ is the mask function. The mask function is equal to one (zero) for $|b| > 30^\circ$ ($|b| < 30^\circ$). In the case of masked point sources, we also have $m(p) = 0$ when a *Fermi* point source is inside the pixel or within two PSF from the boundary of the pixel. We also subtract the average of the data within the unmasked region in order to avoid a non-trivial contribution from a constant source inside the window. We choose the normalization such that for the Poisson noise $\langle C_l \rangle = 1$.

The algorithm for estimating the component that varies on large scales is as follows:

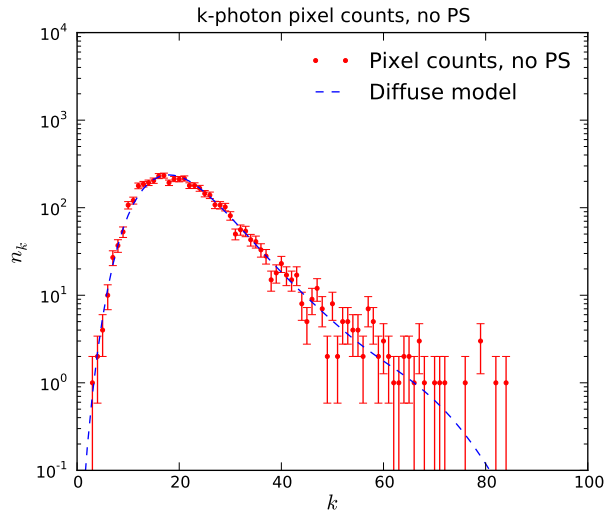


Fig. 7.— Photon counts vs smooth model with *Fermi* point sources subtracted. The Galactic diffuse emission model is obtained by taking the spherical harmonics of the data with $\ell \leq 20$. The model photon counts are derived from the probability generating function in Equation (16) with x_{diff} given in Equation (B2).

1. Calculate the a_{lm} 's inside a window larger than needed (in order to avoid edge effects). We use $|b| > 20^\circ$ for the data above 30° . We also fill in the pixels with point sources by the average of nearest neighbors.
2. The large-scale distribution of gamma-rays is defined as

$$x_{\text{diff}}(p) = A \sum_{l=0}^{l_{\text{max}}} \sum_{m=-l}^l a_{lm} Y_{lm}(p) + B, \quad (\text{B2})$$

where we find the coefficients A and B from the best fit of the diffuse model to the photon counts in the pixels without point sources (see Figure 7).

3. We represent $B = B_{\text{min}} + x_{\text{isotr}}$ so that

$$x_{\text{Gal}}(p) = A \sum_{l=0}^{l_{\text{max}}} \sum_{m=-l}^l a_{lm} Y_{lm}(p) + B_{\text{min}} \quad (\text{B3})$$

is non-negative for $|b| > 30^\circ$. In fitting to full data, A and B_{min} are fixed, while x_{isotr} is allowed to vary together with parameters describing the AGN-like point sources.

An example of the diffuse emission model $x_{\text{diff}}(p)$ for $l_{\text{max}} = 20$ is presented in the middle plot of Figure 6. The top plot represents the counts of photons in pixels inside the window $|b| > 30^\circ$ with

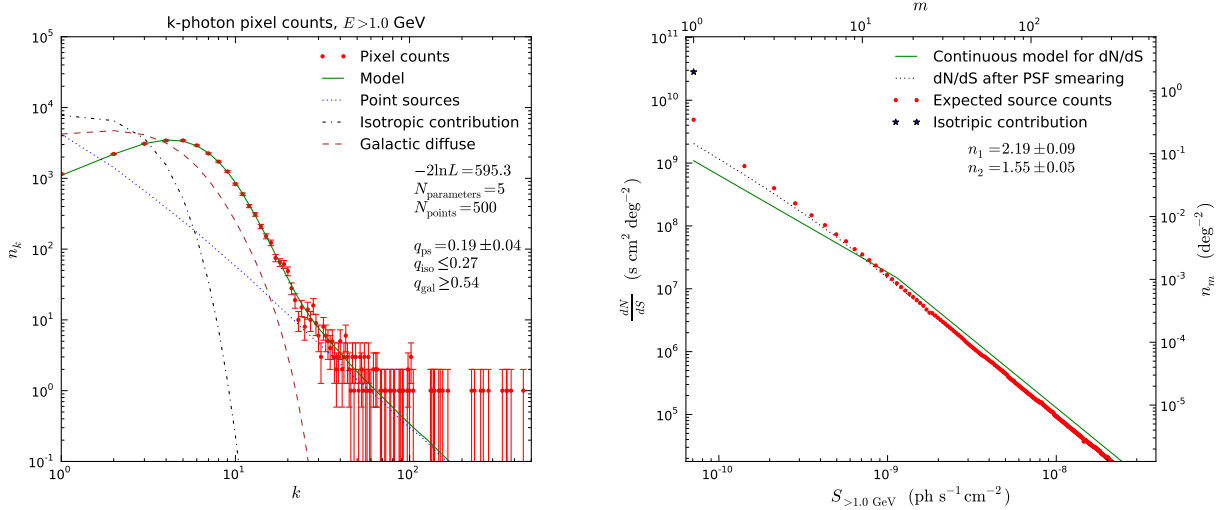


Fig. 8.— Same as in Figure 2 but with the pixel size of about 1° corresponding to HEALPix parameter $\text{nside} = 64$.

masked *Fermi* gamma-ray point sources. The bottom plot represents the deviation of the model from the data in “sigma” values. In Figure 4 we study the effect of changing $l_{\text{max}} = 10, 20, 30$. The difference is rather small, i.e., already $l_{\text{min}} = 10$ captures the large-scale distribution of gamma-rays reasonably well.

C. Variation of pixel size

In the data analysis in Section 3, we use the pixel size of about 2° corresponding to HEALPix parameter $\text{nside} = 32$. In this appendix, we repeat the analysis of Section 3 for different sizes of pixels, in particular we consider $\text{nside} = 64$ and $\text{nside} = 16$ corresponding to pixel sizes 1° and 4° respectively.

The results for $\text{nside} = 64$ are presented in Figure 8. The total number of pixels inside the window below and above 30° in latitude is about 25,000, i.e., the statistics of pixel counts is relatively good, but the effect of PSF becomes more significant than in the case of $\text{nside} = 32$. For $\text{PSF} = 0.4^\circ$, less than about 60% of the flux from a source can be inside one pixel. In particular, one can note that the number of sources with small fluxes is about two times larger than in the input model. Nonetheless, in the case of $\text{nside} = 64$ the best-fit model is similar to $\text{nside} = 32$ case. The position of the break, $S_{\text{break}} = 1.1 \times 10^{-9} \text{ ph s}^{-1} \text{ cm}^{-2}$, is somewhat lower than the values in Table 1 but the overall source count distribution (Figure 9) is consistent with the source counts found by *Fermi* collaboration (Abdo et al. 2010a,c).

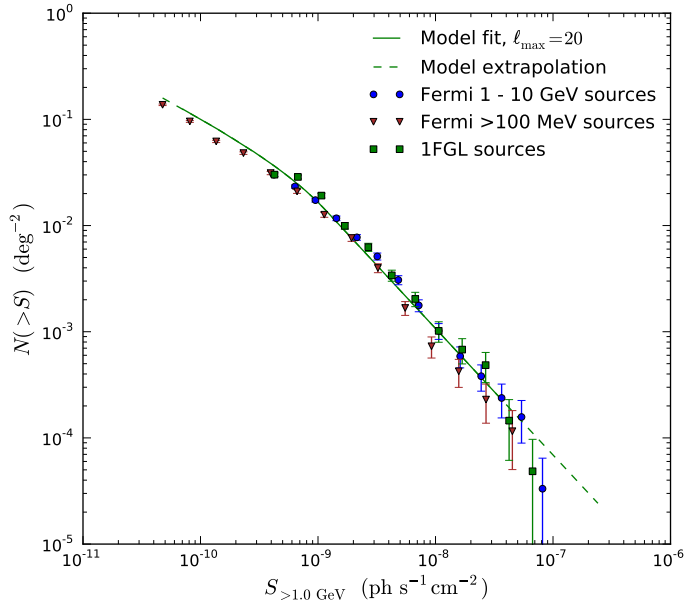


Fig. 9.— Comparison with *Fermi* source counts (Abdo et al. 2010a,c) in the case of analysis with HEALPix parameter $n_{\text{side}} = 64$ (Figure 8).

The results of fitting for $n_{\text{side}} = 16$ are presented in Figure 10. In this case, the PSF can be neglected. However, the number of pixels inside the window is only about 1,500. As one can see on the left side of Figure 10, the error bars are rather large and the photon counts in most of the pixels are dominated by the contribution from diffuse emission. As a result, our method is not sensitive to the contribution from point sources for $n_{\text{side}} = 16$. In particular, the MCMC is dominated by models with large S_{break} . The best fit value $S_{\text{break}} = 1.3 \times 10^{-8} \text{ph s}^{-1} \text{cm}^{-2}$ is an order of magnitude larger than the values in Table 1. The reason is that models with large S_{break} have a comparable likelihood to the models with small S_{break} but there are many more ways to choose a large S_{break} .

We conclude that our method is relatively robust to the change of pixel size: the cases of $n_{\text{side}} = 32$ and $n_{\text{side}} = 64$ give very similar results, unless the number of pixels is not sufficient to draw any conclusion about the statistics of sources, as in the case of $n_{\text{side}} = 16$.

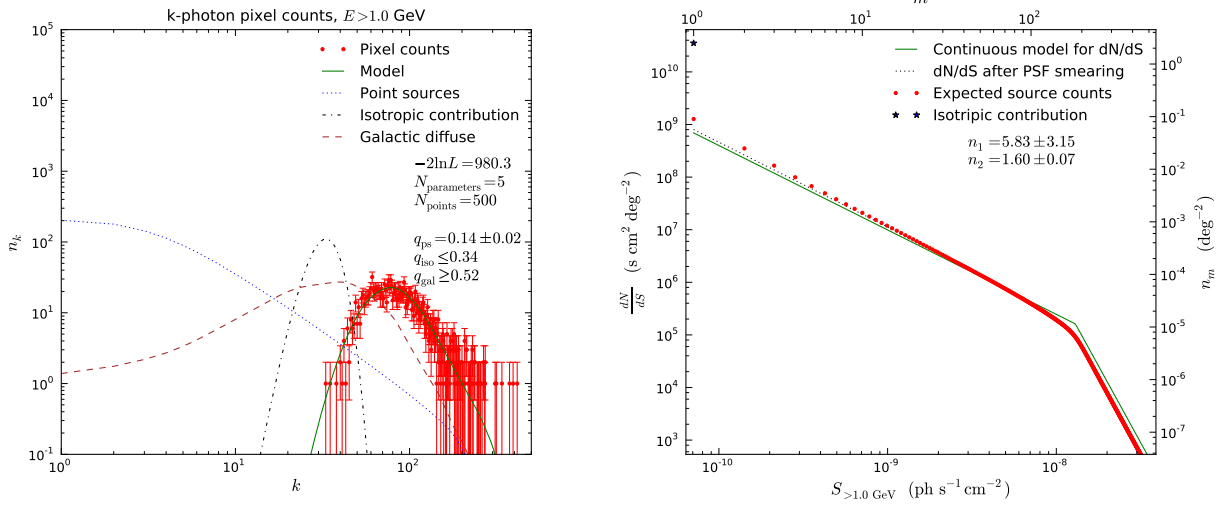


Fig. 10.— Same as in Figure 2 but with the pixel size of about 4° corresponding to HEALPix parameter $n_{\text{side}} = 16$.

REFERENCES

- Abazajian, K. N., Blanchet, S., & Harding, J. P. 2010, arXiv:1012.1247
- Abdo, A. A., et al. 2010a, *ApJS*, 188, 405
- . 2010b, *Physical Review Letters*, 104, 101101
- . 2010c, *ApJ*, 720, 435
- . 2010d, *ApJ*, 716, 30
- Ando, S., & Komatsu, E. 2006, *Phys. Rev. D*, 73, 023521
- Angelakis, E., Fuhrmann, L., Nestoras, I., Zensus, J. A., Marchili, N., Pavlidou, V., & Krichbaum, T. P. 2010, arXiv:1006.5610
- Atwood, W. B., et al. 2009, *ApJ*, 697, 1071
- Ave, M., et al. 2009, *J. Cosmology Astropart. Phys.*, 7, 23
- Berrington, R. C., & Dermer, C. D. 2003, *ApJ*, 594, 709
- Chiang, J., Fichtel, C. E., von Montigny, C., Nolan, P. L., & Petrosian, V. 1995, *ApJ*, 452, 156
- Colombi, S., Davis, O., Devriendt, J., Prunet, S., & Silk, J. 2011, arXiv:1102.5707
- Condon, J. J. 1974, *ApJ*, 188, 279
- Dobler, G., Finkbeiner, D. P., Cholis, I., Slatyer, T., & Weiner, N. 2010, *ApJ*, 717, 825
- Faucher-Giguère, C., & Loeb, A. 2010, *J. Cosmology Astropart. Phys.*, 1, 5
- Fields, B. D., Pavlidou, V., & Prodanović, T. 2010, *ApJ*, 722, L199
- Geringer-Sameth, A., & Koushiappas, S. M. 2010, arXiv:1012.1873
- Górski, K. M., Hivon, E., Banday, A. J., Wandelt, B. D., Hansen, F. K., Reinecke, M., & Bartelmann, M. 2005, *ApJ*, 622, 759
- Hasinger, G., Burg, R., Giacconi, R., Hartner, G., Schmidt, M., Trumper, J., & Zamorani, G. 1993, *A&A*, 275, 1
- Hensley, B. S., Siegal-Gaskins, J. M., & Pavlidou, V. 2010, *ApJ*, 723, 277

- Hodge, J. A., Zeimann, G. R., Becker, R. H., & White, R. L. 2009, *AJ*, 138, 900
- Hoel, P. G., Port, S. C., & Stone, C. J. 1971, *Introduction to Probability Theory* (Boston, MA: Houghton Mifflin)
- Hopkins, P. F., Richards, G. T., & Hernquist, L. 2007, *ApJ*, 654, 731
- Li, F., & Cao, X. 2011, arXiv:1103.4545
- Malyshev, D., Cholis, I., & Gelfand, J. D. 2010, *ApJ*, 722, 1939
- Miyaji, T., & Griffiths, R. E. 2002, *ApJ*, 564, L5
- Mücke, A., & Pohl, M. 2000, *MNRAS*, 312, 177
- Neronov, A., & Semikoz, D. V. 2011, arXiv:1103.3484
- Padovani, P., Ghisellini, G., Fabian, A. C., & Celotti, A. 1993, *MNRAS*, 260, L21
- Padovani, P., & Giommi, P. 1995, *ApJ*, 444, 567
- Padovani, P., Giommi, P., Landt, H., & Perlman, E. S. 2007, *ApJ*, 662, 182
- Pavlidou, V., & Fields, B. D. 2002, *ApJ*, 575, L5
- Rigby, E. E., Best, P. N., & Snellen, I. A. G. 2008, *MNRAS*, 385, 310
- Scheuer, P. A. G. 1957, in *Proceedings of the Cambridge Philosophical Society*, Vol. 53, *Proceedings of the Cambridge Philosophical Society*, 764–773
- Scheuer, P. A. G. 1974, *MNRAS*, 166, 329
- Slatyer, T. R., & Finkbeiner, D. P. 2010, *MNRAS*, 405, 1777
- Smolčić, V., et al. 2009, *ApJ*, 696, 24
- Sołtan, A. M. 2011, arXiv:1101.0256
- Stecker, F. W., & Salamon, M. H. 1996, *ApJ*, 464, 600
- Stecker, F. W., Salamon, M. H., & Malkan, M. A. 1993, *ApJ*, 410, L71
- Stecker, F. W., & Venters, T. M. 2010, arXiv:1012.3678
- Strong, A. W., Moskalenko, I. V., Porter, T. A., Jóhannesson, G., Orlando, E., & Digel, S. W. 2009, arXiv:0907.0559

Strong, A. W., Moskalenko, I. V., & Ptuskin, V. S. 2007, Annual Review of Nuclear and Particle Science, 57, 285

Thompson, T. A., Quataert, E., & Waxman, E. 2007, ApJ, 654, 219

Urry, C. M., & Padovani, P. 1995, PASP, 107, 803